Direct Observation of Dark Excitons in Micelle-Wrapped Single-Wall Carbon Nanotubes

Hideo Kishida,* Yoshiaki Nagasawa, Sadanobu Imamura, and Arao Nakamura
Department of Applied Physics, Nagoya University, Furo-cho, Chikusa-ku, Nagoya 464-8603 Japan
(Received 22 May 2007; published 6 March 2008)

We have performed electroabsorption spectroscopy on micelle-wrapped single-wall carbon nanotubes. In semiconducting nanotubes, many oscillating structures composed of the increase and decrease of absorption are observed in the spectra in the region of the first and second absorption bands, E_{11} and E_{22}. The spectral shape is reproduced mainly by the second-derivative curve of the absorption spectrum, which indicates the presence of nearly degenerate bright and dark excitonic states.

DOI: 10.1103/PhysRevLett.100.097401 PACS numbers: 78.67.Ch, 73.22.−f, 78.20.Jq

Single-wall carbon nanotubes (SWNT) show various characteristic properties resulting from their one-dimensional (1D) structure [1]. One-dimensional band structures show divergent joint density of states (DOS) at the edge. However, the strong exciton binding effects in one-dimensional insulators dominate such DOS effects in absorption spectra. Sharp and strong absorption peaks due to quasi-1D excitons result in resonance-enhanced large nonlinear optical responses [2–5]. The excitons in SWNT are classified by the quantum number ν, which are located in the energy regions below the continuum states labeled as E_{11} and E_{22} in Fig. 1. The excitons with $\nu = 1$ can be two-photon accessible and revealed by the two-photon absorption (TPA) spectra obtained by measuring the excitation-wavelength dependence of two-photon excitation luminescence [6,7].

The doubly degenerate nature of the valence and conduction bands results in the nearly degenerate four excitonic states for each ν. Such nearly degenerate excitons are composed of one bright (one-photon allowed) and three dark (one-photon forbidden) excitons. It is theoretically predicted that some dark exciton states can be two-photon accessible [8,9]. The dark exciton state is thought to be located near the bright exciton state and to play an important role in the relaxation process after photoexcitation [10–14]. Although a high magnetic field brightens the dark states using Aharonov-Bohm effects [15], their energy positions and ordering at zero or low field are still open questions. In order to elucidate excited-state structures like dark excitons, we have to obtain spectra of two-photon excited states by nonlinear optical measurements such as TPA, third-harmonic generation, and electroabsorption (EA). The TPA spectra studied by Wang *et al.* [6] and Maultzsch *et al.* [7] revealed that a $\nu = 1$ exciton state is located 0.3 eV above the lowest one-photon allowed exciton ($\nu = 0$), while it failed to identify dark excitons. The study of dark excitons requires low-noise nonlinear spectroscopy with high photon-energy resolution because dark excitons might be located close to the bright excitons.

Given these conditions, EA spectroscopy would be an extremely powerful tool, whereby two-photon excited states can be observed for a wide energy range with high resolution. Indeed, it is very frequently adopted in the study of excited-state structures in 1D insulators such as conjugated polymers [16,17] and 1D Mott-Hubbard insulators [18]. In the case of SWNT, two papers are devoted to EA measurements; however, the two-photon states are not revealed [19,20]. Theoretical studies suggest that EA measurements in SWNT are quite informative because the Franz-Keldysh or Fano effects may be observed on continuum bands [8,21,22]. In this Letter, we report the EA spectra in the 0.7–3.0 eV range, covering the first and second absorption bands of semiconducting SWNT. Our detailed spectral analysis reveals that the dark excitons are nearly degenerate with the bright excitons in most tubes and located on the slightly higher side of bright excitons in some tubes.

We used the micelle-wrapped SWNT embedded in a transparent host material, gelatin. The SWNT-gelatin film is obtained by a method similar to that described by Kim *et al.* [23] A heated mixture of gelatin solutions and the HiPCO (high-pressure CO) SWNT wrapped with sodium dodecylbenzene sulfonate (SDBS) is dropped onto heated

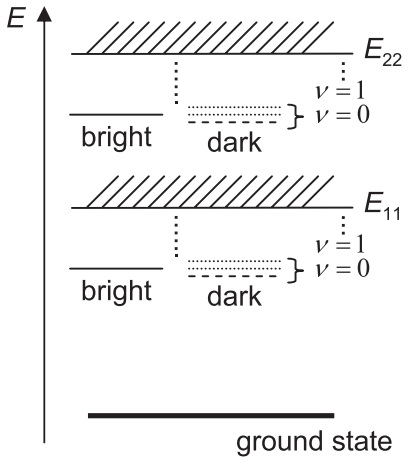

FIG. 1. Schematics of continuum bands and the exciton levels in single-wall carbon nanotubes. One (broken) of the three dark excitons is two-photon allowed states and the others (dotted) are two-photon forbidden ones. The positions of the states are not exact.

ITO/SiO_2 substrates (45 °C). After drying, we obtained a 59-μm-thick film. Aluminum is evaporated onto the SWNT/gelatin films for a semitransparent electrode (thickness of aluminum is 20 nm). An alternating electric field (frequency $f = 1$ kHz) is applied between the Al electrode and ITO. Si and InGaAs photodetectors are used for the EA measurements. The doubled-frequency ($2f$) component (ΔT) of intensity (T) of the transmitted light through the sample is picked up by a lock-in amplifier. The experimentally obtained $-\Delta T/T$ is proportional to the change of absorption ($\Delta\alpha$), namely, $-\Delta T/T \propto \Delta\alpha$ when $|\Delta T/T|$ is small. All the EA spectra are measured at room temperature. The resolution in photon energy is less than 3 meV at 1.0 eV.

The absorption spectra measured at room temperature are shown in Figs. 2(a) and 2(d). Between 0.7 and 1.4 eV, many peaks are observed, which correspond to the transitions assigned to excitons accompanying E_{11} transitions. The peaks between 1.4 and 2.3 eV are assigned to excitons accompanying E_{22} transitions. The transitions above 2.3 eV are assigned to the band-to-band transitions (M_{11}) of metallic tubes. Each peak is ascribed to a different chirality [24,25]. The possible chiral indices (m, n) are indicated in Figs. 2(a) and 2(d). Figures 2(c) and 2(f) show the EA spectra measured at 500 V (85 kV/cm). Between 0.7 and 1.4 eV, the maximum values of the EA signal reach -8×10^{-5}. In the region of E_{22} transitions, the intensities of EA signals are 1 order of magnitude lower than those in the E_{11} region.

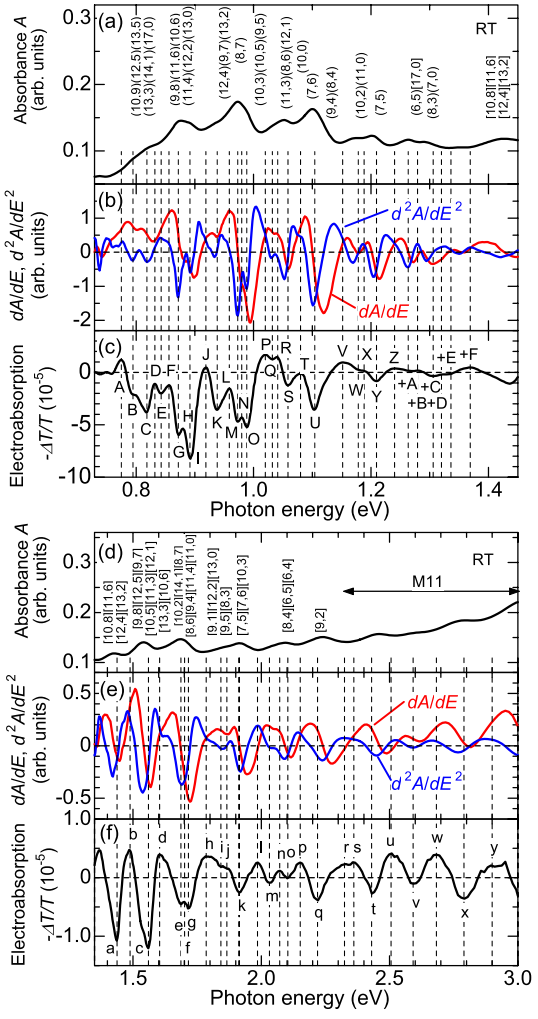

FIG. 2 (color online). (a),(d) Absorption spectra of micelle-wrapped SWNT embedded in gelatin films measured at room temperature. Comparison of EA signals [(c) and (f)] with the first and second-derivative curves ((b) and (e)) of absorption spectra [(a) and (d)]. The possible chiral indices are also shown (round brackets: E_{11} peaks; square brackets: E_{22}). The valley and peak positions in the EA spectra are labeled in (c) and (f) and indicated by vertical broken lines.

In conventional semiconductors, EA signals are often explained by the Franz-Keldysh (FK) effect [26,27], which is the electric-field induced effect on continuum absorption bands. According to the FK model, the spectral shapes depend on the magnitude of the applied electric field in higher field regions. In order to check the contribution from the continuum bands, we measured the electric-field dependence of the EA spectra [Figs. 3(a) and 3(b)]. The spectral shapes remain the same over the whole photon-energy range. Moreover, the intensities of EA signals for all the peaks are proportional to the square of the electric field, as shown in Fig. 3(c). These facts rule out the possibility that the obtained EA spectrum comes from the electric-field effect on the continuum states. All the results reported here indicate that the EA spectra should be ascribed to the electric-field effects on discrete levels such as exciton states. This is consistent with previous reports evidencing excitons [6,7,28–30].

The electric-field effects on discrete excitonic states can be described by the Stark shift. The shift of each level is

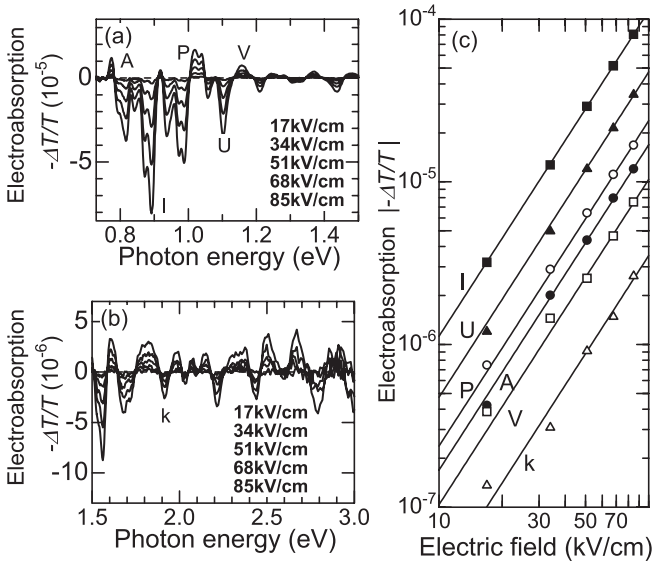

FIG. 3. Electric-field dependence of the EA spectra in the (a) E_{11} and (b) E_{22} regions. (c) The peak intensities of signals at several labeled peaks are plotted as a function of the electric field. The lines with a slope of 2 are a guide to the eye. The labels are the same as those of Fig. 2.

proportional to the square of the electric field. The spectral shape should be approximated by the first derivative of the absorption spectrum. We compare the EA spectrum and the first derivatives in Figs. 2(b) and 2(e). Clearly, some structures such as K, L, P, Q, R, S, W, $+C$, and g appear at the same energy positions as in the first derivatives, but these are minor structures. Next, we compare the EA spectrum and the second derivatives. This comparison reveals that the second derivatives reproduce more peaks and valleys; the energy positions of valleys such as B, C, G, I, M, O, U, Y, $+A$, a, c, e, k, m, q, t, υ, and x are very close to those of the second derivatives. Thus, the agreement of the valley structures and positions is quite good for most nanotubes with different chiral indices. This fact assures that the valleys in EA are not contingent artifacts such as the linear combinations of first derivative curves for various nanotubes but intrinsic structures. Indeed, the valley U, which is composed of the contribution only from (7,6) tubes, is roughly reproduced by the second-derivative curve. This strongly indicates that the second-derivative-like EA spectrum is inherent to SWNT.

We now discuss in more detail the spectral shapes taking into account one-photon allowed and forbidden states. Theoretical studies have predicted two types of one-photon forbidden excitons for SWNT [8,9]. One is the higher states of excitonic series, which have a larger quantum number ($\nu \geq 1$) of excitons. The other one-photon forbidden states are dark excitons, located close to the bright excitons. The excitonic effect in SWNT mixes the doubly degenerate band-to-band transitions to form four split exciton states [10]. These four exciton states have nearly the same envelope functions of excitons, so that all four exciton states belong to the same quantum number of excitons. Importantly, only one of the four exciton states is a ''bright state'', which is accessible from the ground state by one-photon excitation (Fig. 1). The other three states are called ''dark states'' [9,10,12,13]. In *chiral* SWNT, in which $(m - n) = 3p + 1$ or $3p + 2$ (p: integer), one of the three dark excitons is accessible by two-photon excitation, while the other two dark states are neither one- nor two-photon allowed states. In *zigzag* tubes, whose index is $(m, 0)$, all three dark states are forbidden for one- and two-photon excitations. Two-photon allowed states can be observed in EA experiments because the applied electric field can be regarded as zero-frequency photons. According to the above discussion, it is plausible that the Stark shift of one-photon allowed bright exciton and the electric field induced absorption of the two-photon allowed exciton (dark exciton for one-photon excitation) in chiral tubes are observed simultaneously.

The sample used in this study is an ensemble system consisting of nanotubes with various chiral indices. Each nanotube is isolated and the mixing of electronic states between adjacent nanotubes is negligible. Then, overall nonlinear optical responses of the sample should be described by the linear combinations of the contributions from each nanotube. The optical response of each nanotube is dominated by the discrete excitonic levels. In this case, the nonlinear optical processes on each nanotube can be described by the three-state model consisting of the ground state, a one-photon allowed excitonic state, and a two-photon allowed excitonic state. Therefore, we simulate EA spectra using a three-level model composed of a one-photon allowed *bright* exciton (ω_1) and a two-photon allowed *dark* exciton (ω_2). Within this model, the main terms of linear susceptibility, $\chi^{(1)}$, which is related to absorption and third-order nonlinear susceptibility, $\chi^{(3)}$, which is related to EA, are given by [31]

$$\chi^{(1)} = \frac{Ne^2}{\varepsilon_0 \hbar} \frac{\mu_{10}^2}{\omega_1 - \omega - i\gamma_1}, \tag{1}$$

$$\chi^{(3)} = \frac{Ne^4}{3\varepsilon_0 \hbar^3} \frac{\mu_{21}^2 \mu_{10}^2}{(\omega_1 - \omega - i\gamma_1)^2(\omega_2 - \omega - i\gamma_2)}. \tag{2}$$

Here, N is the density of electrons, ω the photon energy, and $\omega_{1(2)}$, $\mu_{10(21)}$, $\gamma_{1(2)}$ are the exciton energy, the transition dipole moment between state 1 and the ground state (state 2) and the damping energy, respectively. Using the linear and nonlinear susceptibilities, we calculated the dielectric constant under the electric field E by the formula $\varepsilon = \varepsilon_1 + i\varepsilon_2 = \varepsilon_0\{1 + \chi^{(1)} + 3\chi^{(3)}E^2\}$. Then, the absorption coefficient α is obtained by the equation $\alpha = \omega\varepsilon_2/cn$ (c: the velocity of light, n: refractive index). The absorption spectrum calculated using $\omega_1 = 1.00$ eV and $\gamma_1 = 0.005$ eV is shown in Fig. 4(a). The first and second derivatives of the absorption spectrum are shown in Fig. 4(b). In the calculation of EA spectra, we vary the positions of dark states from 0.98 to 1.05 eV. The shapes of simulated EA ($\Delta\alpha$) spectra are similar to those of $\mathrm{Im}\chi^{(3)}$ spectra because the EA spectra can be approximated by the expression $\Delta\alpha \approx (3\omega E^2/cn)\mathrm{Im}\chi^{(3)}$. For a degenerate case ($\omega_2 = 1.00$ eV, splitting $\omega_2 - \omega_1 = 0$), the simulated EA spectrum is coincident with the second-derivative curve of absorption. In cases where the dark exciton state is located on a lower (higher) energy side than the bright exciton state, the valley also shifts toward the lower (higher) energy side, as shown in Fig. 4(c). When the dark state ($\omega_2 = 1.05$ eV) is outside the line width, the EA spectrum around the bright exciton is reproduced by a first derivative curve, and the dark state gives a Lorentzian peak at 1.05 eV. Thus, the Stark shift of one-photon states and induced absorption of two-photon states give second-derivative curves only when the bright and dark excitons are degenerated.

The above calculation indicates that the second-derivative feature observed in the experimental EA spectra is due to the degeneracy of dark and bright excitons. Most of the valley positions in the EA spectra coincide with the second derivatives (valleys B, C, G, I, M, O, $+A$, e, k, m, and υ). However, closer scrutiny reveals that some valley positions in the experimental results, such as U, Y, a, c, and x, are slightly higher than those in the second derivatives, and valleys q and t (metallic) are lower. Thus, most peaks deviating from the second derivatives have shifted to higher energies, which indicates that the two-photon al-

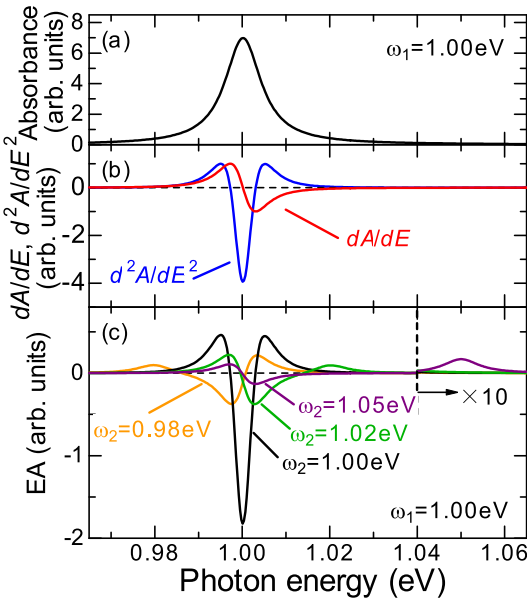

FIG. 4 (color online). Simulated spectra based on three discrete level models composed of the ground state, the bright state fixed at 1.00 eV, and a two-photon state. (a) Absorption spectrum. The damping energy is 5 meV. (b) The first and second-derivative spectra of absorption. (c) EA spectra.

lowed dark excitons are located at higher energies than the bright excitons in some tubes. The upward deviation of the dark excitons from the bright excitons can be roughly estimated by the separation between the dip (negative peak) in the second derivatives of absorption, which gives the position of bright exciton, and the higher positive peak in the EA spectrum such as V for U and Z for Y. The energy separation gives the upper limit of splitting between bright and dark excitons, and its values are approximately 30–50 meV. These values are larger than those estimated by Mortimer *et al.* (1 to 6 meV) from the temperature dependence of luminescence intensity, and the direction of the shift is the opposite [14]. However, we note that there are three dark excitons. The one observed by us is the two-photon allowed dark state, while the one reported by Mortimer *et al.* is related to the lowest dark state governing the relaxation processes.

Apart from the lowest exciton states accompanying the E_{11} and E_{22} bands, which are discussed above, higher exciton states ($\nu \geq 1$) presumably exist. In our results, however, most oscillating structures in the EA spectrum can be accounted for by the first and second derivatives. No clear evidence of higher exciton states is obtained. This can be explained as follows. The intensity of EA signals is governed by two factors: (i) transition dipole moments between one- and two-photon allowed excited states and (ii) the energy separation between them. In the case of the nearly degenerate dark and bright excitons, the transition dipole moments between them may be small [9]. However, the degeneracy leads to a triple resonance, which is easily understood from Eq. (2). The triple resonance enhances the EA signals dramatically and leads to the selective detection of a set of nearly degenerate bright and dark excitons. On the other hand, the EA signal for two-photon allowed states with $\nu \geq 1$ is not detected because the multiresonance mechanism does not work for such states.

In summary, we measured the EA spectra in micelle-wrapped SWNT. The spectra obtained are mainly reproduced by the second-derivative curves of the absorption spectrum. This strongly indicates that dark excitons are nearly degenerate with bright excitons in most tubes. A detailed spectral analysis reveals that the experimental EA spectra deviate slightly from the second derivatives for some tubes. This implies that the dark excitons are on the higher energy side of the bright excitons. Thus, we have clearly observed dark excitons and located their energy positions.

*kishida@nuap.nagoya-u.ac.jp

[1] S. Reich, C. Thomse, and J. Maultzsch, *Carbon Nanotubes* (Wiley-VCH, Weinheim, 2004).
[2] V. A. Margulis and T. A. Sizikova, Physica (Amsterdam) **245B**, 173 (1998).
[3] M. Ichida *et al.*, Physica (Amsterdam) **323B**, 237 (2002).
[4] J-S. Lauret *et al.*, Appl. Phys. Lett. **85**, 3572 (2004).
[5] A. Maeda *et al.*, Phys. Rev. Lett. **94**, 047404 (2005).
[6] F. Wang *et al.*, Science **308**, 838 (2005).
[7] J. Maultzsch *et al.*, Phys. Rev. B **72**, 241402(R) (2005).
[8] E. B. Barros *et al.*, Phys. Rev. B **73**, 241406 (2006).
[9] H. Zhao *et al.*, Phys. Rev. B **73**, 075403 (2006).
[10] H. Zhao and S. Mazumdar, Phys. Rev. Lett. **93**, 157402 (2004).
[11] C. D. Spataru *et al.*, Phys. Rev. Lett. **95**, 247402 (2005).
[12] Y. -Z. Ma *et al.*, Phys. Rev. B **74**, 085402 (2006).
[13] B. C. Satishkumar *et al.*, Phys. Rev. B **74**, 155409 (2006).
[14] I. B. Mortimer and R. J. Nicholas, Phys. Rev. Lett. **98**, 027404 (2007).
[15] S. Zaric *et al.*, Science **304**, 1129 (2004).
[16] L. Sebastian and G. Weiser, Chem. Phys. **62**, 447 (1981).
[17] M. Liess *et al.*, Phys. Rev. B **56**, 15712 (1997).
[18] H. Kishida *et al.*, Nature (London) **405**, 929 (2000).
[19] C. Gadermaier *et al.*, Nano Lett. **6**, 301 (2006).
[20] T. Takenobu, Y. Murayama, and Y. Iwasa, Appl. Phys. Lett. **89**, 263510 (2006).
[21] V. Perebeinos and P. Avouris, Nano Lett. **7**, 609 (2007).
[22] H. Zhao and S. Mazumdar, Phys. Rev. Lett. **98**, 166805 (2007).
[23] Y. Kim, N. Minami, and S. Kazaoui, Appl. Phys. Lett. **86**, 073103 (2005).
[24] S. M. Bachilo *et al.*, Science **298**, 2361 (2002).
[25] R. B. Weisman and S. M. Bachilo, Nano Lett. **3**, 1235 (2003).
[26] M. Cardona, *Modulation Spectroscopy* (Academic, New York, 1969).
[27] D. E. Aspnes and J. E. Rowe, Phys. Rev. B **5**, 4022 (1972).
[28] T. Ando, J. Phys. Soc. Jpn. **66**, 1066 (1997).
[29] M. Ichida *et al.*, J. Phys. Soc. Jpn. **68**, 3131 (1999).
[30] M. Freitag *et al.*, Nano Lett. **3**, 1067 (2003).
[31] P. N. Butcher and D. Cotter, *The Elements of Nonlinear Optics* (Cambridge University Press, Cambridge, England, 1990).